Stringent limits on top-quark compositeness from $t\bar{t}$ production at the Tevatron and the LHC

M. Fabbrichesi,[1] M. Pinamonti,[2] and A. Tonero[3]

[1]*Sezione di Trieste, INFN, 34136 Trieste, Italy*
[2]*Gruppo collegato di Udine, Sezione di Trieste, INFN and SISSA, via Bonomea 265, 34136 Trieste, Italy*
[3]*ICTP South American Institute for Fundamental Research & Instituto de Física Teórica, UNESP, Rua Dr. Bento T. Ferraz 271, 01140-070 São Paulo, São Paulo, Brazil*

(Received 19 September 2013; published 11 April 2014)

If the top quark is a composite state made out of some constituents, then its interaction with the gluon will be modified. We introduce the leading effective operators that contribute to the radius and anomalous magnetic moment of the top quark and study their effect on the cross section for $t\bar{t}$ production at the Tevatron and the LHC. Current measurements of the cross sections set a stringent limit on the scale of compositeness. This limit is comparable to similar limits obtained for light quarks and those from electroweak precision measurements. It can be used to constrain the parameter space of some composite Higgs models.

DOI: 10.1103/PhysRevD.89.074028 PACS numbers: 14.65.Ha, 12.60.Rc, 13.85.Lg

I. MOTIVATIONS

Whether the top quark is a point-like particle or an extended object is a question that can now be addressed thanks to the large number of them produced at the LHC and the Tevatron. The most recent, combined measurement of the cross section for $t\bar{t}$ production is in good agreement with the most up-to-date theoretical prediction within the standard model (SM) and this result can be used to put constraints on the compositeness of the top quark.

Whereas in the SM the top quark—as well as all other fundamental particles—has no structure, various extensions of the SM are based on some form of compositeness: in particular, the composite Higgs boson [1,2], as well as its partial compositeness implementation [3,4], but also models inspired by the littlest Higgs [5] and technicolor [6] assume the existence of a strongly interacting sector, the SM particles being either composite objects themselves or mixing with particles which are. The top quark, being the heaviest of all states, is the best candidate for searching for possible signatures of such compositeness. The problem has been previously addressed in [7] and more recently in [8–15]. We discuss in some detail the implications of the limits we find on possible extensions to the SM in the last section.

A. Composite top quark and strong interactions

Compositeness can manifest itself in various ways. We take the most direct approach and look into what effect a finite extension of the top quark has on its interaction with the gauge bosons. In the case most relevant for collider physics, we can write two form factors $F_1(q^2)$ and $F_2(q^2)$ modifying the vertex between the top quark and the gluon as

$$g_s \bar{t}\left[\gamma^\mu F_1(q^2) + \frac{i\sigma^{\mu\nu}q_\nu}{2m_t}F_2(q^2)\right]G_\mu t, \tag{1}$$

where g_s is the strong $SU(3)_C$ coupling constant, $G_\mu = T_A G_\mu^A$ is the gluon field, T_A are the $SU(3)_C$ group generators, q^μ is the momentum carried by the gluon, t denotes the top-quark field and $\sigma^{\mu\nu} = i[\gamma^\mu, \gamma^\nu]/2$. The interaction in eq. (1) is the most general after assuming that the vector-like nature of the gluon-top–quark vertex is preserved by the underlying dynamics giving rise to the composite state.

As originally pointed out for the case of electromagnetic interactions [16], the physics of the form factors in eq. (1) is best represented by the combinations

$$G_E(q^2) = F_1(q^2) + \frac{q^2}{4m_t^2}F_2(q^2) \quad \text{and}$$
$$G_M(q^2) = F_1(q^2) + F_2(q^2), \tag{2}$$

which are (in the Breit frame) the Fourier transform of, respectively, the chromoelectric and chromomagnetic charge densities ρ_c and $\mu\rho_m$ of, in our case, the top quark. For an extended object these densities are not Dirac δ-functions and can be expanded. To the leading order, we thus obtain a first momentum (the chromomagnetic moment μ),

$$G_M(q^2) = \frac{2}{\pi}\int dr r^2 j_0(qr)\mu\rho_m(r) \simeq \mu + \cdots, \tag{3}$$

from the chromomagnetic charge density, and a second momentum (the squared mean radius $\langle\vec{r}^2\rangle$),

$$G_E(q^2) = \frac{2}{\pi}\int dr r^2 j_0(qr)\rho_c(r) \simeq 1 - \frac{\vec{q}^2}{6}\langle \vec{r}^2\rangle + \cdots, \quad (4)$$

from the chromoelectric charge density. In Eqs. (3)–(4), $j_0(x) = \sin x/x$ represents the spherical Bessel function of order zero and the (nonrelativistic) charges ρ_c and ρ_m are related to the four-current as

$$j^\mu(r) = (g_s\rho_c(r), \mu\vec{\sigma}\times\vec{\nabla}\rho_m(r)). \quad (5)$$

The two parameters μ and $\langle\vec{r}^2\rangle$ are traditionally used in nuclear physics to characterize the finite extension of nucleons and other extended objects.

Form factors are just a way of organizing the perturbative expansion. An alternative and perhaps better approach is effective field theory. In this language the expansion is given in terms of operators invariant under the underlying symmetries that are added to the SM Lagrangian. These operators have a dimension higher than four and are suppressed by negative powers of the new physics scale to get the required dimension.

In this work we use the effective field theory approach and consider the contributions given by $SU(3)_C \times U(1)_{em}$ invariant effective operators to the top-quark form factors introduced in eq. (1). The leading contributions come from the following two higher dimensional operators:

$$\hat{O}_1 = g_s\frac{C_1}{m_t^2}\bar{t}\gamma^\mu T_A t D^\nu G^A_{\mu\nu} \quad \text{and}$$
$$\hat{O}_2 = g_s\frac{C_2 v}{2m_t^2}\bar{t}\sigma^{\mu\nu}T_A t G^A_{\mu\nu}, \quad (6)$$

where $D^\nu G^A_{\mu\nu} = \partial^\nu G^A_{\mu\nu} + g_s f^A{}_{BC} G^{\nu B} G^C_{\mu\nu}$, $G^A_{\mu\nu} = \partial_\mu G^A_\nu - \partial_\nu G^A_\mu + g_s f^A{}_{BC} G^B_\mu G^C_\nu$ is the gluon field strength tensor, $f^A{}_{BC}$ are the $SU(3)_C$ structure constants and $v = 174$ GeV is the electroweak (EW) symmetry breaking vacuum expectation value. In eq. (6) the operators $\hat{O}_1$ and $\hat{O}_2$ are, respectively, of the dimension six and five. We limit ourselves to the CP-conserving case and the dimensionless coefficients C_1 and C_2 are taken to be real. Left- and right-hand fermion fields enter symmetrically. The operator $\hat{O}_1$ gives the leading q^2 dependence to F_1 while $\hat{O}_2$ gives the q^2-independent term of F_2:

$$F_1(q^2) = 1 + C_1\frac{q^2}{m_t^2} + \ldots \quad \text{and} \quad F_2(0) = 2C_2\frac{v}{m_t}. \quad (7)$$

Operators of higher dimensions can in general contribute—they give further terms in the expansion of the form factors—but their effect should be suppressed. We have checked that possible corrections due to dimension eight operators, such as

$$G_{\mu\nu}G^{\mu\nu}\bar{q}\,\tilde{H}\,t_R, \quad (8)$$

are suppressed as long as the coefficients are taken to be $O(C^2_{1,2})$.

The form of the coefficients in front of the operators in eq. (6) is conventional and dictated, in our case, by the analogy with the electromagnetic form factors. In addition, the operator $\hat{O}_2$ is written for convenience with an extra factor v/m_t because it can be thought as coming, after EW symmetry breaking, from a dimension six $SU(3)_C \times SU(2)_L \times U(1)_Y$ gauge invariant operator that includes the Higgs boson field.

Replacing the expressions of the form factors obtained in eq. (7) into eq. (2), we can obtain an estimate of the radius and chromomagnetic moment of the top quark using the same formulas that apply in the electromagnetic case. We have that

$$\langle\vec{r}^2\rangle = -6\left.\frac{dG_E}{d\vec{q}^2}\right|_{q^2=0} \quad \text{and} \quad \mu = G_M(0), \quad (9)$$

where μ is the chromomagnetic moment of the top quark measured in units of $g_s/2m_t$.

The aim of this work is to give an estimate of the size of these quantities by constraining the values of the dimensionless coefficients C_1 and C_2 using the available LHC public data on the $t\bar{t}$ total production cross section $\sigma(pp \to \bar{t}t)$ and those for the $\sigma(p\bar{p} \to \bar{t}t)$ from the Tevatron. In addition, we also include constraints from data on spin correlations of the top quarks at the LHC. The results will be used in the last section where we will translate the bounds on C_1 and C_2 into limits on new physics scales in the framework of some specific models.

The finite extension of the source generating the terms in eq. (9) arises because of the radiative corrections of the parton-level processes as well as because of the presumed compositeness. In order to disentangle these two contributions we assume that the former is included in the SM cross section computed at the next-to-leading order (NLO) and beyond [for the most recent exact computation at the next-to-next-to-leading order (NNLO) and next-to-next-to-leading logs (NNLL), see [17] and citations therein], leaving C_1 and C_2 to encode only effects intrinsically due to compositeness.

The operators $\hat{O}_1$ and $\hat{O}_2$ enter at tree level into the computation of the $t\bar{t}$ production cross section through gluon fusion and quark-antiquark annihilation. The first channel is the dominant one at the LHC while the second is dominant at the Tevatron. At tree level, in addition to the usual SM QCD Feynman diagrams, one has to take into account the contributions coming from the new interactions as depicted in Fig. 1 and Fig. 2. The diagram (f) of Fig. 1 is a contribution not present in the SM and is due to the presence of the operators $\hat{O}_1$ and $\hat{O}_2$; it represents the effective interaction of two gluons and the $\bar{t}t$ pair. Notice that the contribution of the operator $\hat{O}_1$ cancels out in the sum of the gluon fusion amplitudes.

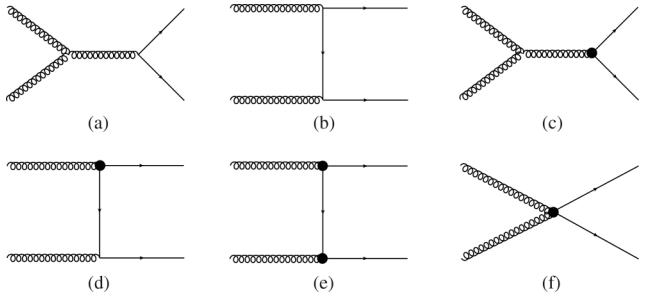

FIG. 1. Parton-level Feynman diagrams for the process $gg \to \bar{t}t$. This process dominates at the LHC. The blob represents the insertion of either the operator $\hat{O}_1$ or $\hat{O}_2$.

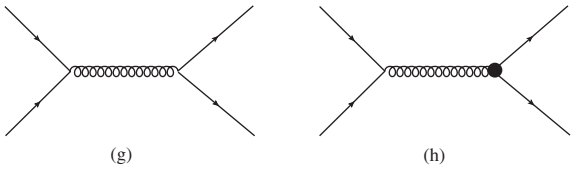

FIG. 2. Parton-level Feynman diagrams for the process $qq \to \bar{t}t$. This process dominates at the Tevatron. The blob represents the insertion of either the operator $\hat{O}_1$ or $\hat{O}_2$.

Following the effective field theory approach, one has to write down all possible dimension five and six operators that contribute to the $t\bar{t}$ production cross section. It is possible to show [18] that—by rearrangement and field redefinitions using the equations of motion—out of all possible operators that contribute to this process only three are independent, namely $\hat{O}_1$, $\hat{O}_2$ in eq. (6) and a set of four-fermion operators. If we further assume the same coefficient in front of the four-fermion operators involving two top quarks and two light quarks of different flavors, then these four-fermion operators too can be rewritten, by means of the equations of motion, in terms of the operator $\hat{O}_1$. We are thus left with just the two operators $\hat{O}_1$ and $\hat{O}_2$ in eq. (6). Notice that in general, the whole set of four-fermion operators entering in the dimension six SM effective Lagrangian is larger and cannot be rewritten as O_1.

Anomalous couplings and top-quark production has been discussed by several authors [11], most recently in [12] (and [13], which came out while we were finishing this work). The anomalous magnetic moment of these references corresponds to the coefficient C_2 of the chromomagnetic operator in eq. (6). Ref. [14] follows an approach similar to ours but with different and less stringent results. The effect on $\bar{t}t$-production of $\hat{O}_2$ (together with the four-fermion operators) has been studied in [15] in the context of nonresonant new physics at the Tevatron and the LHC. See [19] for an updated version.

In the low-energy regime, data on B-physics can be affected by the operators in eq. (6). In particular, the operator O_2 contributes to the matching condition of the Wilson coefficient of the chromomagnetic operator between the quark b and s. The latter operator mixes with the electromagnetic dipole moment operator

$$em_b\bar{b}\sigma^{\mu\nu}(1+\gamma_5)sF_{\mu\nu}, \tag{10}$$

which gives rise to the transition $b \to s\gamma$. Even though data on the branching fraction [20] can in principle be used to set limits on the coefficient C_2, the estimates in literature give either too small an effect [21] or one with large uncertainties [22]. For this reason, we do not use these limits.

II. METHODS

A. Monte Carlo implementation

In order to study new physics effects on $t\bar{t}$ production cross sections (and spin correlations) at the LHC and Tevatron, we have first used FeynRules [23] to implement our model, which has been defined to be the SM with the addition of the two effective operators $\hat{O}_1$ and $\hat{O}_2$ of eq. (6). FeynRules provides the universal FeynRules output (UFO) with the Feynman rules of the model. The UFO is then used by MadGraph 5 [24] (MG5) to compute the production cross section that we denote by $\sigma_{\mathrm{MG5}}(C_1, C_2)$.

The main $t\bar{t}$ production channel at LHC is given by gluon fusion and the associated Feynman diagrams are those in Fig. 1. Other subleading channels are given by quark-antiquark annihilation, whose diagrams are depicted in Fig. 2. MG5 computes the square of the amplitude for each single channel and then convolutes the result with the probability distribution functions (pdf) of the partons inside the proton in order to obtain the total $pp \to t\bar{t}$ production cross section. The default set of pdf used is CTEQ6L1.

The partonic level result thus obtained can be compared with the partonic experimental cross section that is extracted by the experimental collaborations from the fully hadronized cross section—which is what is actually measured at the colliders.

We compute, using MG5, $\sigma_{\mathrm{MG5}}(C_1, C_2)$ for three different values of the center-of-mass energy (7, 8 and 14 TeV), varying the absolute values of both C_1 and C_2 in a range that goes from 0 to 0.1. These different values of $\sigma_{\mathrm{MG5}}(C_1, C_2)$ will be used to obtain limits on the coefficients C_1 and C_2 by comparing the MG5 computation with the measured cross section at the center-of-mass (CM) energy $\sqrt{s} = 7$ and 8 TeV and the expected result at 14 TeV, as discussed in the next section.

By proceeding in the same way, we have also computed the $t\bar{t}$ production cross section at the Tevatron and compared it with the measured cross section at the CM energy $\sqrt{s} = 1.98$ TeV. In this case, the main $t\bar{t}$ production channel is given by quark-antiquark annihilation and the associated Feynman diagrams are those depicted in Fig. 2. As we shall see, in this case we obtain a particular stringent bound on C_1.

B. Statistical analysis

The quantity used to obtain 95% confidence level (C.L.) limits on the coefficients C_1 and C_2 is the cross section $\Delta\sigma_{\rm exp}$, which is defined to be the difference between the central value of the measured cross section $\bar{\sigma}_{\rm exp}$ and that of the SM theoretical value $\bar{\sigma}_{\rm th}$:

$$\Delta\sigma_{\rm exp} = \bar{\sigma}_{\rm exp} - \bar{\sigma}_{\rm th}. \tag{11}$$

The uncertainty is given by summing in quadrature the respective uncertainties:

$$\sqrt{(\delta\sigma_{\rm exp})^2 + (\delta\sigma_{\rm th})^2}. \tag{12}$$

Using the cross sections $\sigma_{\rm MG5}(C_1, C_2)$ calculated with MG5, we compute the value of the cross section coming from new physics $\Delta\sigma_{\rm MG5}(C_1, C_2)$ as

$$\Delta\sigma_{\rm MG5}(C_1, C_2) = \sigma_{\rm MG5}(C_1, C_2) - \sigma_{\rm MG5}(0, 0). \tag{13}$$

The quantity $\Delta\sigma_{\rm MG5}(C_1, C_2)$ represents the contribution to the cross section coming from the interference between the SM leading order and new physics diagrams. Terms coming from the interference between new physics and higher order QCD diagrams are not included in this approximation.

Values of C_1 and C_2 for which $\Delta\sigma_{\rm MG5}(C_1, C_2)$ is more than two standard deviations from $\Delta\sigma_{\rm exp}$, namely

$$\Delta\sigma_{\rm MG5}(C_1, C_2) > \Delta\sigma_{\rm exp} + 2\sqrt{(\delta\sigma_{\rm exp})^2 + (\delta\sigma_{\rm th})^2}, \tag{14}$$

or

$$\Delta\sigma_{\rm MG5}(C_1, C_2) < \Delta\sigma_{\rm exp} - 2\sqrt{(\delta\sigma_{\rm exp})^2 + (\delta\sigma_{\rm th})^2}, \tag{15}$$

can be considered excluded at 95% C.L.

III. RESULTS

A. SM cross section

A typical one-loop radiative correction to the vertices gives a contribution to the top-quark radius $O(\alpha_s/2\pi m_t^2)$. Because the effect of compositeness is of the same order, the SM theoretical amplitude $\sigma_{\rm th}$ used for obtaining the exclusion limits, as explained in the previous section, must contain at least NLO contributions which include these corrections as well as those coming from initial and final state radiation.

Production of top-quark pairs at hadron colliders is a challenging computation that has been pursued for many years and is now available at the NNLO [17]. In addition, the soft gluon re-summation for the same process is known at the NNLL order necessary for the matching [25]. Following [17] we take, for a top-quark mass of 172.5 GeV, the following values for the cross section at the LHC for, respectively, the CM energy $\sqrt{s} = 7$ and 8:

$$\sigma_{\rm th}(pp \to t\bar{t}) = \begin{cases} 176.25^{+4.6}_{-5.9}\,({\rm scale})^{+4.8}_{-4.9}\,({\rm pdf})\ {\rm pb}\ ({\rm LHC@7}) \\ 251.68^{+6.4}_{-8.6}\,({\rm scale})^{+6.3}_{-6.5}\,({\rm pdf})\ {\rm pb}\ ({\rm LHC@8}) \end{cases}, \tag{16}$$

where the first uncertainty is due to the residual scale dependence and the second to the pdf of the partons which are taken from the MSTW200NNLO68CL set [26]. At the Tevatron, for a CM energy $\sqrt{s} = 1.98$ TeV, the same reference [17] gives

$$\sigma_{\rm th}(p\bar{p} \to t\bar{t}) = 7.35^{+0.11}_{-0.21}\,({\rm scale})^{+0.17}_{-0.12}\,({\rm pdf})\ {\rm pb}\ ({\rm Tevatron}). \tag{17}$$

The size of the overall uncertainty of these results—summing the square of the two errors—is a substantial improvement with respect to the NLO result.

B. Current data and bounds: LHC and Tevatron

The cross section for the production of top-quark pairs has been measured at LHC and Tevatron for its respective energy range.

The best current measurements at the LHC of the cross section $\sigma_{\rm exp}(pp \to \bar{t}t)$ combining the various channels at the CM energy of $\sqrt{s} = 7$ TeV, for a top-quark mass of 172.5 GeV, is

$$\sigma_{\rm exp}(pp \to t\bar{t}) = \begin{cases} 177.0 \pm 3\,({\rm stat})^{+8}_{-7}\,({\rm syst}) \pm 7\,({\rm lumi})\ {\rm pb}\ ({\rm ATLAS}) \\ 165.8 \pm 2.2\,({\rm stat}) \pm 10.6\,({\rm syst}) \pm 7.8\,({\rm lumi})\ {\rm pb}\ ({\rm CMS}) \end{cases} \tag{18}$$

for, respectively, the ATLAS [27] and the CMS [28].

A combination of ATLAS and CMS results is available [29] for an integrated luminosity of up to 1.1 fb^{-1}:

$$\sigma_{\rm exp}(pp \to \bar{t}t) = 173.3 \pm 10.1\ {\rm pb}\ ({\rm LHC@7}), \tag{19}$$

with an overall uncertainty of 5.8% which we will use in our analysis to set the limits.

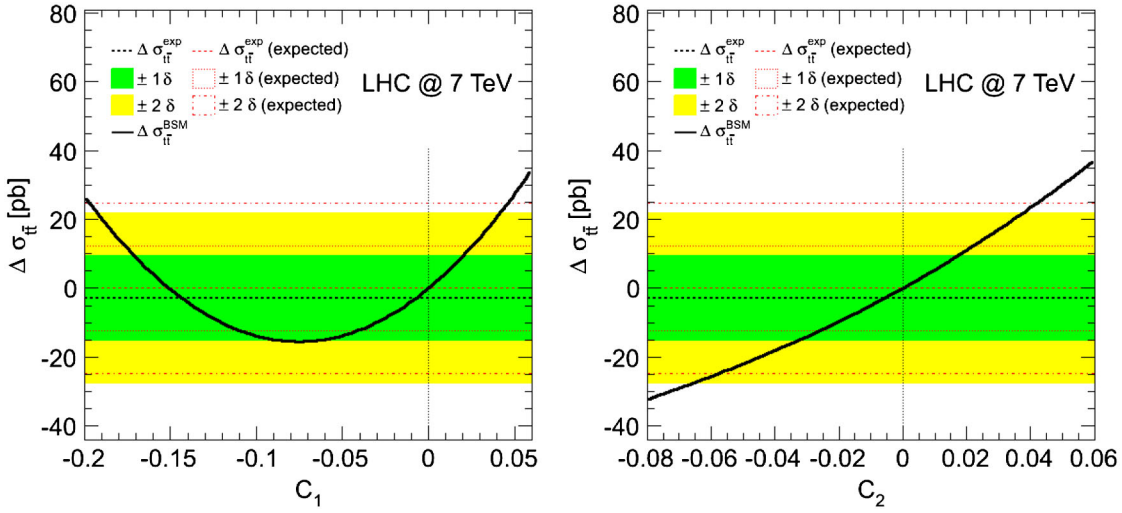

FIG. 3 (color online). Constraints on the coefficients C_1 and C_2 from data at the LHC at $\sqrt{s} = 7$ TeV. On the left is the limit on C_1 with $C_2 = 0$. On the right is the limit on C_2 with $C_1 = 0$. The horizontal dashed black line represents the experimental central value. The yellow (green) band represents $2(1)\sigma$ uncertainties. The red lines are the expected limits at 1 and 2σ level. The thick black line is the cross section in the presence of the new operators at sampled values of the coefficients C_i.

Figure 3 show the limits coming from LHC@7 on the coefficients C_1 and C_2 obtained by means of the above experimental result and the theoretical computation in eq. (16).

In Fig. 3, as well as in the following figures, the black line with dots represents the cross section $\Delta\sigma_{\mathrm{MG5}}$ which includes the contributions of the operators $\hat{O}_1$ and $\hat{O}_2$. The yellow (green) bands represent the cross section $\Delta\sigma_{\mathrm{exp}}$ with its error at the $2(1)\sigma$ level. Finally, the horizontal red lines represent the expected limits (at the 1 and 2σ levels) which are obtained by identifying the central value of the experimental data $\bar{\sigma}_{\mathrm{exp}}$ with the central value of the theoretical prediction $\bar{\sigma}_{\mathrm{th}}$.

The best current measurements of the cross section $\sigma_{\mathrm{exp}}(pp \to \bar{t}t)$ at the CM energy of $\sqrt{s} = 8$ TeV for a top-quark mass of 172.5 GeV is

$$\sigma_{\mathrm{exp}}(pp \to t\bar{t}) = \begin{cases} 237 \pm 1.7\,(\mathrm{stat}) \pm 7.4\,(\mathrm{syst}) \pm 7.4\,(\mathrm{lumi}) \pm 4.0\,(\mathrm{beam\ energy})\ \mathrm{pb}\ \ (\mathrm{ATLAS}) \\ 227 \pm 3\,(\mathrm{stat}) \pm 11\,(\mathrm{syst}) \pm 10\,(\mathrm{lumi})\ \mathrm{pb}\ \ (\mathrm{CMS}) \end{cases} \tag{20}$$

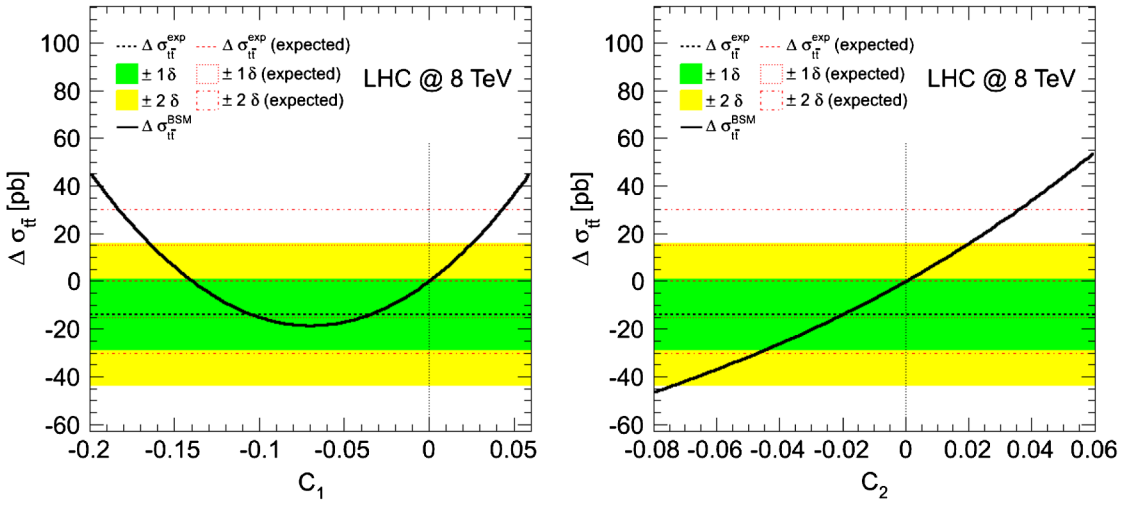

FIG. 4 (color online). Constraints on the coefficients C_1 and C_2 from data at the LHC at $\sqrt{s} = 8$ TeV. On the left is the limit on C_1 with $C_2 = 0$. On the right is the limit on C_2 with $C_1 = 0$. The horizontal dashed black line represents the experimental central value. The yellow (green) band represents $2(1)\sigma$ uncertainties. The red lines are the expected limits at the 1 and 2σ levels. The black line is the cross section in the presence of the new operators at sampled values of the coefficients C_i.

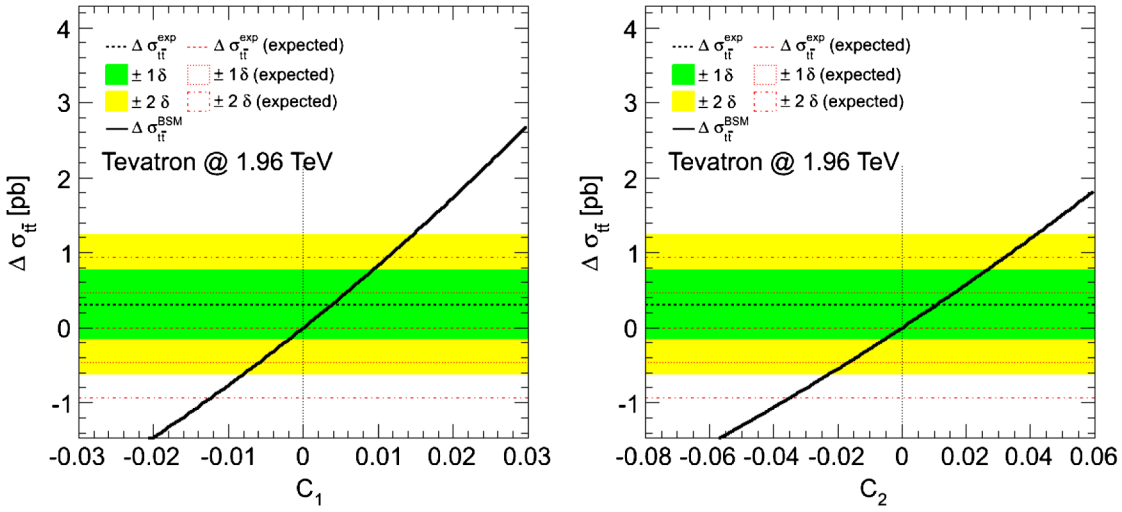

FIG. 5 (color online). Constraints on the coefficients C_1 and C_2 from data at the Tevatron at $\sqrt{s} = 1.96$ TeV. On the left is the limit on C_1 with $C_2 = 0$. On the right is the limit on C_2 with $C_1 = 0$. The horizontal dashed black line represents the experimental central value. The yellow (green) band represents $2(1)\sigma$ uncertainties. The red lines are the expected limits at the 1 and 2σ levels. The black line is the cross section in the presence of the new operators at sampled values of the coefficients C_i.

for, respectively, an integrated luminosity of 5.8 fb^{-1} at ATLAS [30] and 2.4 fb^{-1} at CMS [31], in both cases considering events with dilepton final states.

Lacking a combined value, we consider the experimental value of ATLAS [30], which has smaller uncertainties, to set the limits; the theoretical value is taken from eq. (16). Figure 4 shows the result in this case. Notice that improved limits with respect to the previous ones at $\sqrt{s} = 7$ TeV are mainly due to the lower central value of the experimental data. This is made clear by the comparison with the expected C.L. (the red horizontal lines in Fig. 4).

Combined data from CDF and D0 at the Tevatron [32] give the following cross section at the CM energy of $\sqrt{s} = 1.96$ TeV up to an integrated luminosity of 8.8 fb^{-1}:

$$\sigma_{\text{exp}}(p\bar{p} \to \bar{t}t) = 7.65 \pm 0.42 \text{ pb (Tevatron)}. \quad (21)$$

Figure 5 shows the limits coming from Tevatron on the coefficients C_1 and C_2 we obtain by means of the above experimental result and the theoretical computation in eq. (17). The data from the Tevatron are particularly stringent in the case of the operator $\hat{O}_1$ because of the

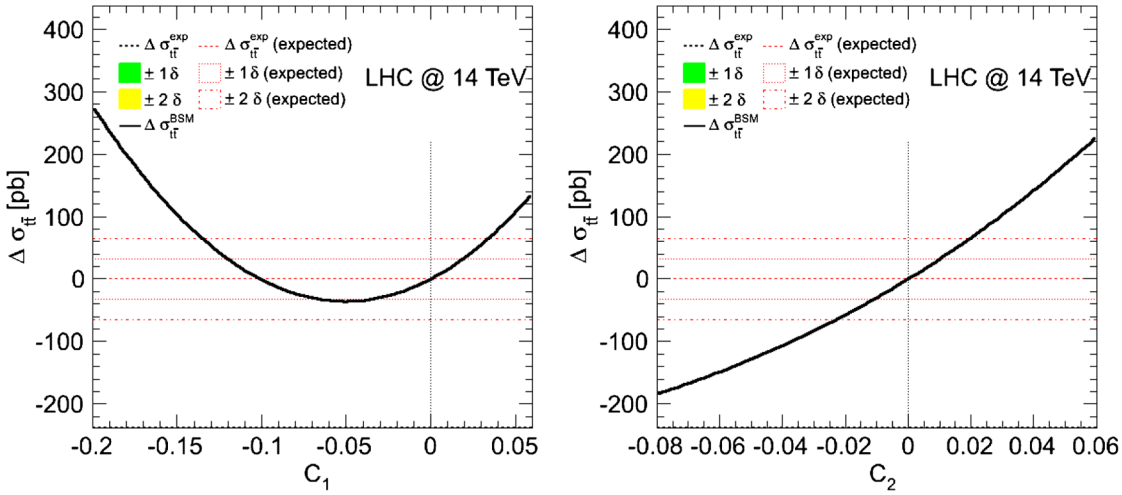

FIG. 6 (color online). Possible constraints on the coefficients C_1 and C_2 from data at the LHC at $\sqrt{s} = 14$ TeV. On the left is the limit on C_1 with $C_2 = 0$. On the right is the limit on C_2 with $C_1 = 0$. The horizontal dashed red line represents the experimental central value. The other red lines are the expected limits at the 1 and 2σ levels. The black line is the cross section in the presence of the new operators at sampled values of the coefficients C_i.

kinematical configuration that prefers the $qq \to t\bar{t}$ channel which is, in turn, most sensitive to that operator.

C. Future bounds: LHC at $\sqrt{s} = 14$ TeV

If we assume that the experimental uncertainty will remain around 5%—it is difficult to imagine doing better than this—we can plot the expected limits at the LHC when the CM energy will be $\sqrt{s} = 14$ TeV by fixing the experimental central value to coincide with the theoretical cross section:

$$\sigma_{\rm th}(p\bar{p} \to t\bar{t}) = 953.6^{+22.7}_{-33.9}\,({\rm scale})^{+16.2}_{-17.8}\,({\rm pdf})\ {\rm pb} \times ({\rm LHC@14})\ [17]. \quad (22)$$

As depicted in Fig. 6, the increase in energy improves the limits with respect to what was to be expected at the LHC at lower CM energies. However, the study at 14 TeV does not modify in a significative manner the overall limits because the actual experimental value at 8 TeV turned out lower than the theoretical value and therefore yielded a better than expected limit.

D. Differential cross section

Even though the differential cross section for $t\bar{t}$ production contains, in principle, extra information that can be used to set limits on the compositeness of the top quark, we find that the current experimental uncertainties are too large to significantly improve the best limits we found by considering the total cross section.

The best case occurs for the cross section as a function of the invariant mass $m_{t\bar{t}}$ for the LHC with data at $\sqrt{s} = 7$ TeV [33] and for the coefficient C_1. Figure 7 plots this cross section in bins and shows the experimental value with its error and the variation for different values of the coefficient C_1.

To set limits combining the total cross section $\sigma_{\rm tot} = \sigma_{t\bar{t}}$ and the relative differential cross section $\sigma_{{\rm dif},i} = (1/\sigma_{t\bar{t}})d\sigma_{t\bar{t}}/dm_{t\bar{t}}$ in each bin i, we evaluated an χ^2 function as

$$\chi^2 = \left[\frac{\sigma^{\rm exp}_{\rm tot} - \sigma^{\rm th}_{\rm tot}}{\delta(\sigma_{\rm tot})}\right]^2 + \sum_{i=0}^{N_{bins}} \left[\frac{\sigma^{\rm exp}_{{\rm dif},i} - \sigma^{\rm th}_{{\rm dif},i}}{\delta(\sigma_{{\rm dif},i})}\right]^2, \quad (23)$$

where $\delta(\sigma)$ refers to the squared sum of the experimental and the theoretical uncertainties on the respective $\sigma_{\rm tot}$ and $\sigma_{{\rm dif},i}$, and the suffix th refer to the theoretical prediction. This theoretical prediction is given by the NLO + NLL calculation [34] plus the contribution from new physics depending on the value of C_1, evaluating generating events with MADGRAPH and then PYTHIA [35].

This quantity χ^2 is evaluated for each of the considered values of C_1 and compared with a distribution of χ^2 values obtained generating 10^3 pseudoexperiments allowing the measured values to fluctuate following a Gaussian distribution $G(\sigma, \delta(\sigma))$. A value of C_1 was considered excluded at 95% C.L. if less than 5% of the pseudoexperiments resulted in an χ^2 value larger than the one for the given value of C_1.

To get an approximate 95% C.L. exclusion limit on C_1, the obtained values of χ^2 as a function of C_1 were interpolated as shown on the right side of Fig. 7. The dashed horizontal line represents the value $\hat{\chi}^2$ for which $\chi^2 < \hat{\chi}^2$ in 95% of the pseudoexperiments. The limit we find is $C_1 < 0.03$, which is an improvement with respect to what was found from data on the LHC total cross section at the same CM energy, but still less stringent than that found from the Tevatron data for the total cross section.

Direct analysis of the Tevatron data [36] and the LHC at $\sqrt{s} = 8$ TeV [37] yields weaker limits. The effect of the coefficient C_2 on the cross section distributions is negligible because of the experimental uncertainties in the different intervals of $m_{t\bar{t}}$.

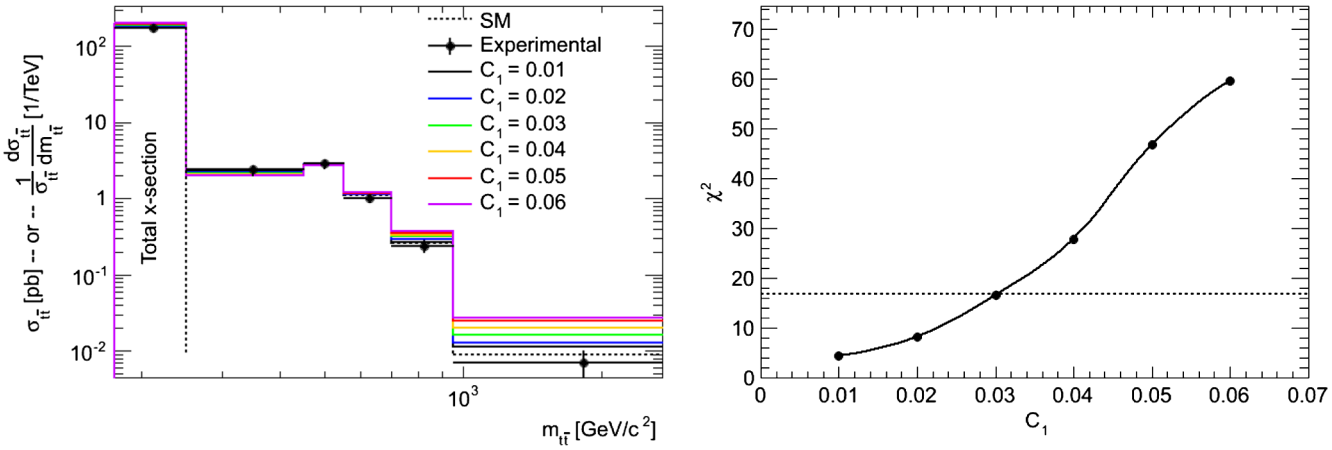

FIG. 7 (color online). Left side: Differential cross section in bins of $m_{t\bar{t}}$ for LHC at 7 TeV. In the first bin is the total cross section. In color are the changes bin by bin for different values of the coefficient C_1. Right side: Limit on the coefficient C_1 (see the text).

E. Spin correlations: LHC at $\sqrt{s} = 7$ TeV

Independent observables useful in setting further limits on the top-quark structure involve spin correlation in $t\bar{t}$ events [38]. Spin correlations of pair-produced top quarks can be extracted by analyzing the angular distributions of the top-quark decay products in $t \to Wb$ followed by the leptonic decay of the W boson $W \to l\nu$. If no acceptance cuts are applied and the spin-analyzing power is effectively 100%, then we have the following form of the double angular distribution [38]:

$$\frac{1}{\sigma}\frac{d^2\sigma}{d\cos\theta_1 d\cos\theta_2} = \frac{1}{4}(1 + B_1\cos\theta_1 + B_2\cos\theta_2 - C_h\cos\theta_1\cos\theta_2), \quad (24)$$

where B_1, B_2 and C_h are coefficients.

Here, we consider the angular distribution in the helicity basis, in which the quantization axes are taken to be the t and $\bar{t}$ directions of flight in the $t\bar{t}$ zero-momentum frame. Therefore, $\theta_1(\theta_2)$ represents the angle between the direction of flight of $l^+(l^-)$ in the $t(\bar{t})$ rest frame and the $t(\bar{t})$ direction of flight in the $t\bar{t}$ zero-momentum frame. In this case the spin correlation coefficient C_h is given by

$$C_h = \frac{N(\uparrow\uparrow) + N(\downarrow\downarrow) - N(\downarrow\uparrow) - N(\uparrow\downarrow)}{N(\uparrow\uparrow) + N(\downarrow\downarrow) + N(\downarrow\uparrow) + N(\uparrow\downarrow)}, \quad (25)$$

where $N(\uparrow\uparrow) + N(\downarrow\downarrow)$ represents the number of events where the top and antitop-quark spin projections are parallel, and $N(\downarrow\uparrow) + N(\uparrow\downarrow)$ is the number of events where they are antiparallel with respect to the chosen quantization axes.

For the experimental analysis it is more convenient to use the one-dimensional distributions of the product of the cosines $O_h \equiv \cos\theta_1 \cdot \cos\theta_2$ and define an asymmetry A_h which, in the absence of acceptance cuts, is determined by [38]

$$A_h = \frac{N(O_h > 0) - N(O_h < 0)}{N(O_h > 0) + N(O_h < 0)} = -\frac{C_h}{4}. \quad (26)$$

The most precise experimental measurement of C_h at LHC is obtained by ATLAS studying at $\sqrt{s} = 7$ TeV the angular separation $\Delta\phi$ between the charged leptons in dileptonic $t\bar{t}$ events [39]:

$$C_h^{\text{meas}} = 0.37 \pm 0.06\,(\text{stat} + \text{syst}). \quad (27)$$

This value has to be compared with the next-to-leading order SM prediction

$$C_h^{\text{NLO}} = 0.31, \quad (28)$$

calculated in [38] including QCD and electroweak corrections to $t\bar{t}$ production and decay.

The spin correlation coefficient C_h as a function of the effective operators coefficients is obtained by means of MG5, generating 10^5 events for the process $pp \to t\bar{t} \to b\ell^+\nu\bar{b}\ell^-\bar{\nu}$, for different values of C_1 and C_2, and computing the asymmetry A_h defined in eq. (26).

MG5 gives a tree level prediction for the total cross section $\sigma(pp \to t\bar{t} \to b\ell^+\nu\bar{b}\ell^-\bar{\nu})$ that we denote by $\sigma^{\text{MG5}}(C_1, C_2)$ and therefore also the derived asymmetry is a LO result that we denote by $A_h^{\text{MG5}}(C_1, C_2)$. The tree level prediction for the asymmetry is then corrected in order to take into account the SM NLO effects by computing

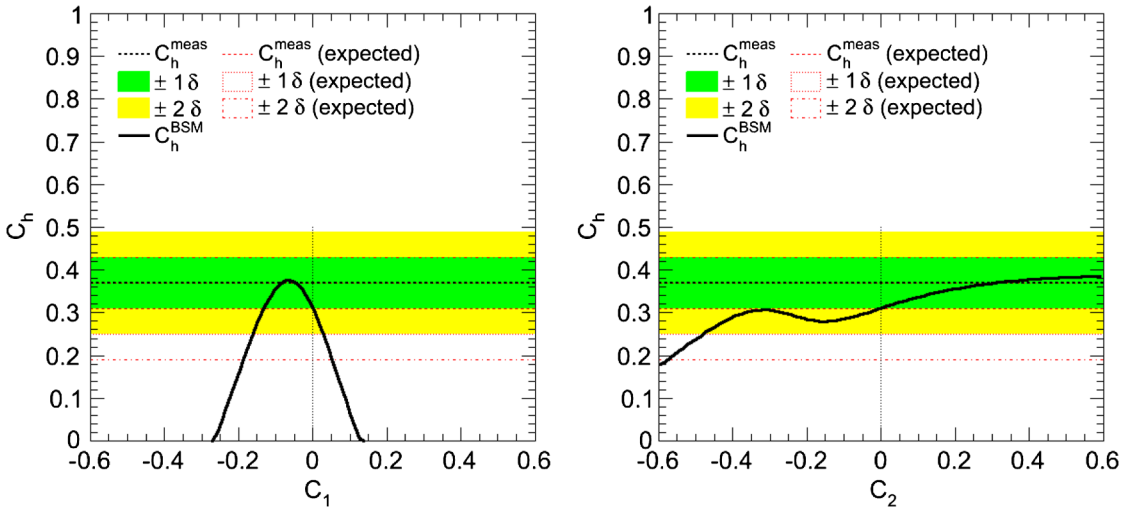

FIG. 8 (color online). Constraints on the coefficients C_1 and C_2 from data on spin correlations at the LHC at $\sqrt{s} = 7$ TeV. On the left is the limit on C_1 with $C_2 = 0$. On the right is the limit on C_2 with $C_1 = 0$. The horizontal dashed black line represents the experimental central value. The yellow (green) band represents $2(1)\sigma$ uncertainties. The red lines are the expected limits at the 1 and 2σ levels. The black line is the asymmetry C_h computed in the presence of the new operators as a function of the coefficients C_i.

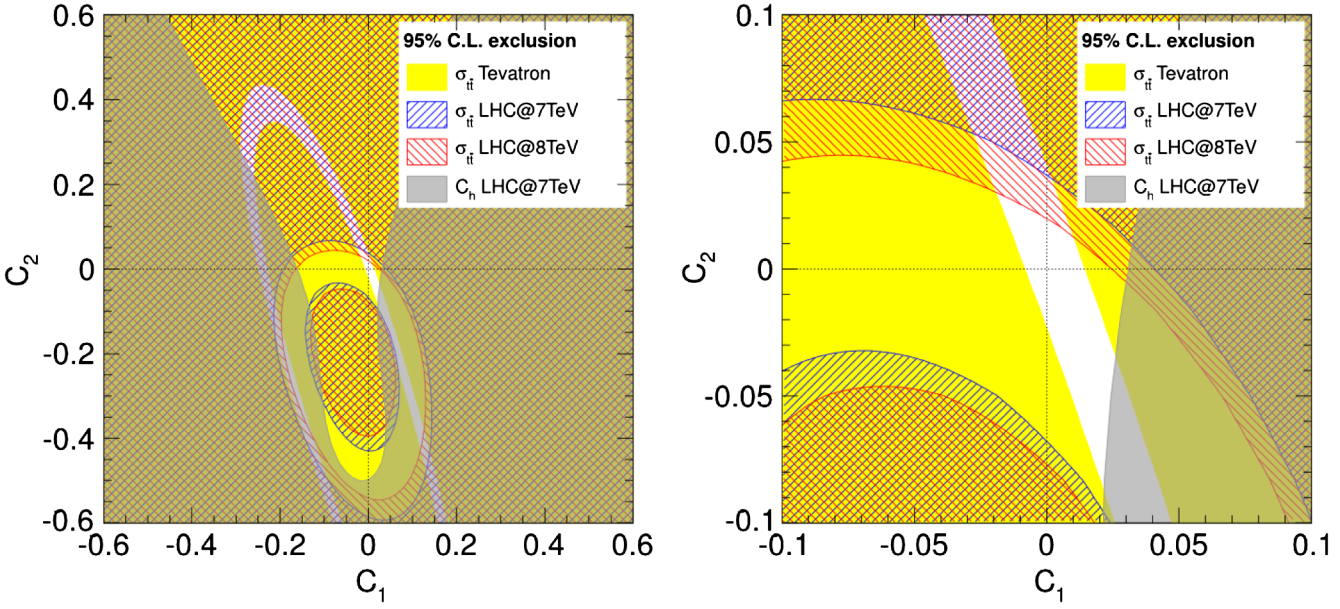

FIG. 9 (color online). Combined limits on the coefficients C_1 and C_2 from data at the LHC ($\sqrt{s} = 8$ and 7 TeV) and Tevatron ($\sqrt{s} = 1.96$ TeV). Values in the regions, respectively, in hatched blue and hatched red from LHC, yellow from Tevatron and gray from spin correlations at the LHC are excluded at 95% C.L. The allowed region corresponds to the white area. On the right is a zoomed plot around the allowed values.

$$A_h(C_1, C_2) = \frac{A_h^{\mathrm{NLO}} \cdot \sigma^{\mathrm{NLO}} + A_h^{\mathrm{MG5}}(C_1, C_2) \cdot \sigma^{\mathrm{MG5}}(C_1, C_2) - A_h^{\mathrm{MG5}}(0,0) \cdot \sigma^{\mathrm{MG5}}(0,0)}{\sigma^{\mathrm{NLO}} + \sigma^{\mathrm{MG5}}(C_1, C_2) - \sigma^{\mathrm{MG5}}(0,0)}, \tag{29}$$

where σ^{NLO} is obtained by multiplying the NNLO theoretical cross section for $t\bar{t}$ production in [17] by the leptonic decay branching ratio and A_h^{NLO} is computed using Eq. (26) from Eq. (28).

Figure 8 shows the limits on the coefficients C_1 and C_2 coming from the spin correlations at the LHC at $\sqrt{s} = 7$ TeV. The black line represents the correlation coefficient computed including the contributions of the operators $\hat{O}_1$ and $\hat{O}_2$ as described above. The yellow (green) bands represent the measured C_h with its error at the $2(1)\sigma$ level. We can see from Fig. 8 that differently to C_1, the coefficient C_2 is unbounded for positive values.

F. Combined limits

The bounds on the individual coefficients C_1 and C_2 can also be computed when both operators are simultaneously present. In this case, there is an important modulation in the effect of the new operators. The combined limits coming from the data at the LHC at the two CM energies considered and those at the Tevatron are shown in Fig. 9. In the same plot, also the limits coming from the spin correlations are shown.

We can see that without the data on the spin correlations the allowed region is rather large. Other analyses [11–15] found a smaller region because they either kept only the leading order contribution of the operators or did not combine the limits on C_2 with those on C_1. When the full contribution of these operators is included for both of them, we need the limits from data on the spin correlations in order to exclude the larger values and obtain relevant limits.

IV. DISCUSSION

We have collected in Table I the limits for the two coefficients C_1 and C_2 when they are varied simultaneously and independently of each other for each of the data sets. Pending results from the LHC at $\sqrt{s} = 14$ TeV, the

TABLE I. Limits on the coefficients C_1 and C_2 when they are varied independently of each other and simultaneously (last column). The starred numbers for LHC@14 are the expected limits.

Tevatron	LHC@7	LHC@8	LHC@14	Combined
$-0.008 \le C_1 \le 0.015$	$-0.193 \le C_1 \le 0.042$	$-0.165 \le C_1 \le 0.025$	$-0.135^\star \le C_1 \le 0.034^\star$	$-0.019 \le C_1 \le 0.026$
$-0.023 \le C_2 \le 0.042$	$-0.066 \le C_2 \le 0.038$	$-0.074 \le C_2 \le 0.020$	$-0.023^\star \le C_2 \le 0.020^\star$	$-0.087 \le C_2 \le 0.031$

Tevatron gives the most stringent bound on the operator $\hat{O}_1$. The LHC at $\sqrt{s} = 8$ TeV and the Tevatron give the best bounds on the operator $\hat{O}_2$. In combining the limits, all data sets are important and those from spin correlations are essential in removing large values for the coefficients C_1 and C_2 which cannot be ruled out by the total cross section data because of cancellations between the two contributions.

A. The size of the top quark

Deviations from the point-like behavior of a particle are usually expressed in terms of charge radius and anomalous magnetic moment. These quantities have been defined in Eq. (3) and Eq. (4). In the case of the top quark the dominant probe is charged under the $SU(3)$ group of strong interactions. Since there is no definite boundary, the size is usually discussed in terms of the root-mean-squared (RMS) radius.

We should first identify the size that comes from radiative corrections. This part is a departure from the point-like behavior due to the cloud of virtual states surrounding any particle in quantum field theory. For the top quark, the leading radiative contribution to the squared mean radius can be computed in perturbation theory to the one-loop order in QCD and it is in general of the order $(\alpha_s/2\pi)1/m_t^2$. Accordingly, this contribution to the RMS radius is about 10^{-5} fm. EW interactions give an additional (smaller) contribution which can be neglected.

We can obtain an estimate of the fraction of the radius and moment of the composite top quark which is not part of the radiative corrections in terms of the effective operator coefficients. Using the formulas in Eq. (7) to compute the form factors of Eq. (2), we have that, using Eq. (9),

$$\langle \vec{r}^2 \rangle = \frac{6}{4}\frac{4m_t C_1 + 2vC_2}{m_t^3} \quad \text{and} \quad \mu = 1 + 2\frac{v}{m_t}C_2, \tag{30}$$

with $2vC_2/m_t$ equal to the anomalous component of the magnetic moment. The best constraints on the coeficients C_1 and C_2 when taken independently,

$$-0.008 \leq C_1 \leq 0.015 \quad \text{and} \quad -0.023 \leq C_2 \leq 0.020, \tag{31}$$

correspond to a RMS radius,

$$\sqrt{\langle \vec{r}^2 \rangle} < 4.6 \times 10^{-4} \text{ fm} \quad (95\%\text{C.L.}), \tag{32}$$

and an anomalous magnetic moment,

$$-0.046 < \mu - 1 < 0.040 \quad (95\%\text{C.L.}). \tag{33}$$

A similar bound on the anomalous magnetic moment of the top quark has been reported in [12]. The bounds found in [14] are weaker. At the time of writing this paper, an apparently stronger bound was found in [13] which however agrees with our limit if taken at the 68% C.L.

These limits become weaker if the constraints are taken simultaneously for the two operators:

$$\sqrt{\langle \vec{r}^2 \rangle} < 7.4 \times 10^{-4} \text{ fm} \quad \text{and} \quad -0.17 < \mu - 1 < 0.062 \quad (95\%\text{C.L.}). \tag{34}$$

To put the above limits in perspective, let us consider the proton and the electron as the best known examples of, respectively, a composite and (presumably) point-like particle.

The radiative part of the proton RMS radius is about 10^{-2} fm. Its actual size, as measured in electron-proton elastic scattering experiments, is much larger: it is about 0.9 fm [40]. The factor of 100 in the ratio of these two numbers is not far from what we have found in the case of the top quark.

The electron, which is believed to be a point-like particle, has a limit on its RMS which does not originate in radiative corrections and that is not far from that in Eq. (32) for the top quark: it is 10^{-5} fm [41]. In other words, the top quark does not seem to deviate from a point-like object down to a scale close to that of the electron. Notice that the bound in the electron case comes from an analysis of $e^+e^- \to e^+e^-$ while in our case that for the top quark comes from $\bar{q}q \to \bar{t}t$ rather than the more direct $\bar{t}t \to \bar{t}t$ which would be probed by the process with four top quarks in the final states. The limit on the part of the electron anomalous magnetic moment not accounted for by radiative corrections is very strong—because of its interaction with a classical magnetic field—and equal to 10^{-12} [42].

B. Compositeness and physics beyond the SM

The most direct way to associate some compositeness scales Λ_1 and Λ_2 to the effect of the operators in Eq. (6) is through the identification

$$\frac{1}{\Lambda_1^2} = \frac{g_s|C_1|}{m_t^2} \quad \text{and} \quad \frac{1}{\Lambda_2^2} = \frac{g_s|C_2|}{2m_t^2}. \tag{35}$$

The identification of Λ_2 in Eq. (35) is based on the full EW symmetry group for which the operator $\hat{O}_2$ must be considered of dimension six. In this way, it is simple to translate the bounds on C_1 and C_2, obtained in the previous section, into limits on these two scales of compositeness. We have that

$$\Lambda_1 > \begin{cases} 1.3 \text{ TeV} & (\text{Tevatron}) \\ 0.4 \text{ TeV} & (\text{LHC@7}) \\ 0.4 \text{ TeV} & (\text{LHC@8}) \end{cases}$$
$$\Lambda_2 > \begin{cases} 1.1 \text{ TeV} & (\text{Tevatron}) \\ 0.9 \text{ TeV} & (\text{LHC@7}) \\ 0.8 \text{ TeV} & (\text{LHC@8}) \end{cases} \quad (95\%\text{C.L.}). \tag{36}$$

These results can be compared with bounds coming from EW precision measurements [43]: the scale of the four-fermion operators (for light quarks) is bounded to values higher, depending on the sign and the procedure, than 6.6 or 9.5 TeV. More generally, by using various other operators an the overall bound of $\Lambda > 17$ TeV is found.

While the above identification of the compositeness scale is straightforward—it plays the role of expansion parameter for the operators—its link to specific models is more indirect.

In the following sections we discuss how to translate bounds on C_1 and C_2 into limits on the parameters of two models of physics beyond the SM. In doing so, we must bear in mind that often numerical values, when used within a given model, are more orders of magnitude than precise numbers because both naive power counting and the QCD analogy may not be correct in a generic strongly interacting theory.

1. Contact interactions

Contact interactions are usually introduced to parametrize generic models of compositeness [44]. These have been traditionally described by the interaction

$$\frac{2\pi}{\Lambda_{\rm CI}^2}\bar{\psi}_L\gamma^\mu\psi_L\bar{\psi}_L\gamma_\mu\psi_L, \tag{37}$$

where $\psi = (ud)^T$ and $\Lambda_{\rm CI}$ is identified as the contact interaction scale. The factor of 2π is conventional and suggested by a strongly interacting sector, the coupling of which is assumed to be $g^2 \simeq 2\pi$. Under such an assumption, the effective four-fermion operator can be thought as generated by the exchange of a heavy resonance, which couples to the fermion with strength g, and that has been integrated out. The effect of four-fermion operators with light quarks in $\sigma(pp \to jj + X)$ was first discussed in [44] and more recently in [45,46].

Performing a field redefinition, using the equations of motion for the gluon field, it is possible to rewrite the operator $\hat{O}_1$ as a combination of four-fermion interaction terms:

$$\hat{O}_1 = \frac{g_s^2 C_1}{m_t^2}\bar{t}\gamma_\mu T_A t\sum_q \bar{q}\,\gamma^\mu T^A q, \tag{38}$$

where the summation runs over all quark species. Assuming contact interactions which are flavor universal, we can directly relate the contribution of the operator $\hat{O}_1$ to that in Eq. (37). By taking into account color factors, flavor and chirality multiplicity, we have the following identification:

$$\Lambda_{\rm CI} = \sqrt{\frac{6\pi}{g_s^2 C_1}}m_t. \tag{39}$$

The constraints on the coefficients C_1 therefore apply to this scale and give

$$\Lambda_{\rm CI} > \begin{cases} 5.0\ \text{TeV} & \text{(Tevatron)} \\ 1.4\ \text{TeV} & \text{(LHC@7)} \\ 1.5\ \text{TeV} & \text{(LHC@8)} \end{cases} \quad (95\%\text{C.L.}), \tag{40}$$

respectively.

For recent bounds on the characteristic scale of these operators from measurements of dijets at the LHC, see [47]. In these references, $\Lambda_{\rm CI}$ in Eq. (37) is found to be around 10 TeV in the case of light quarks. The limits (40) coming from the top quark are less stringent but of the same order of magnitude.

2. Strongly interacting light Higgs models

Strongly interacting light Higgs models (SILH) are theories in which the Higgs multiplet is assumed to belong to a new (strong) sector responsible for the EW symmetry breaking [9]. These models are broadly characterized by two parameters, a coupling constant g_* and a scale m_*, which denotes the mass of the heavy physical states.

The leading new physics effects are parametrized in terms of dimension six operators, involving the Higgs and the other SM fields, consistent with $SU(3)_C \times SU(2)_L \times U(1)_Y$ symmetry. Among these operators, we are interested in the following one:

$$c_{tG}\bar{q}_L H^c\sigma^{\mu\nu}T_A t_R G^A_{\mu\nu} + \text{h.c.}, \tag{41}$$

where $q^T = (tb)$ and $H^c = i\sigma^2 H^*$ is the conjugated Higgs field. The size of the coefficients of these effective operators is usually derived by naive dimensional analysis (NDA) [48] as described in [9,19].

Naive estimation of the coefficient c_{tG} in Eq. (41) gives $c_{tG} \sim g_s y_t/m_*^2$. After EW symmetry breaking, the operator in Eq. (41) reduces to the operator $\hat{O}_2$ of Eq. (6) with the identification

$$|C_2|/2m_t^2 = y_t/m_*^2. \tag{42}$$

In this way we can translate the bounds on C_2 into limits on the mass m_*. By using the results of the previous section we find

$$m_\star > \begin{cases} 1.2\ \text{TeV} & \text{(Tevatron)} \\ 0.9\ \text{TeV} & \text{(LHC@7)} \\ 0.9\ \text{TeV} & \text{(LHC@8)} \end{cases} \quad (95\%\text{C.L.}). \tag{43}$$

A special phenomenological realization of SILH is represented by theories where the Higgs doublet is a composite Goldstone boson of a spontaneously broken symmetry of the strong dynamics [1,2]. In these models the ratio $m_*/g_* \equiv f$ is identified with the decay constant of the

Goldstone boson associated with the symmetry breaking. An important quantity of these composite models is the ratio $\xi = v^2/f^2$, which characterizes the distance between the EW and the strong dynamics scales.

How the scale $m_\star$ should be properly interpreted within the composite models depends on whether the assumption of minimal coupling is taken as a guiding principle or not. For a recent discussion and criticism about this point, see [49].

If we assume the strongly interacting theory to be minimally coupled, then the coupling of the composite top quark to the gluon field remains the same as for the SM fermions. Accordingly, the operator in Eq. (41) can be generated only at loop level—by means of the coupling to the heavier resonances—and the coefficient c_{tG} receives a further suppression by a factor of $g_*^2/16\pi^2$. In this case, while it is possible to obtain a bound on the scale f—because of the identification $|C_2|/2m_t^2 = y_t/16\pi^2 f^2$—and therefore on the parameter ξ, the constraints we have found are too weak to bound the parameter space of these models.

On the other hand, if the interaction with the gluon field of the composite top quark is assumed to be nonminimal, which is the most reasonable assumption for a composite object, then we can start out directly with the interaction vertexes in Eq. (1) and m_* can be taken to coincide with the mass of the heavy composite fermion. The result holds both in the case of complete and partial compositeness. A specific model of partial compositeness in which this scenario is realized is discussed in Appendix A.

In composite models, both the right-hand and left-hand top quark should have a sizable degree of compositeness. The right-hand top quark t_R could be completely composed; there are no experimental limits beside those discussed here. The compositeness of the left-hand top quark t_L is more constrained because of its pairing with the b quarks in an $SU(2)$ doublet and the experimental constraints from the decay $Z \to b\bar{b}$. However, it is possible to show [50] how to protect b_L from corrections in such a decay, thus leaving open the possibility of its being a composite state as well.

In the case of the composite Higgs models, the composite fermion masses must be close to the scale f [10,51] in order for the Higgs boson mass to be equal to its experimental value. If we assume a nonminimal coupling scenario, following the discussion above, it is possible to identify $m_\star \simeq f$ in Eq. (42). In this case the parameter ξ is accordingly constrained to be

$$\xi < \begin{cases} 0.04 & \text{(Tevatron)} \\ 0.07 & \text{(LHC@7)} \\ 0.08 & \text{(LHC@8)} \end{cases} \quad (95\%\text{C.L.}). \tag{44}$$

Notice that values of ξ below 0.1 require a high degree of cancellation between different terms in order to keep the Higgs boson mass at its experimental value and are therefore considered unnatural and make the usefulness of the model doubtful.

In considering the above constraints, we must bear in mind that there are many caveats depending on the connection in a specific model between the composite states and the top quark. Most notably, in models with partial compositeness [3,4] further suppression factors—making the above limits weaker—may come from the mixing angles between heavy composite and light states, as shown in a specific model in Appendix A. The same model also shows that while the limits in Eq. (44) can be slightly relaxed, they cannot be made substantially weaker.

An independent limit on the scale f can be obtained by means of the operator $\hat{O}_1$, which, using the equations of motion, gives rise to the four-fermion operator of Eq. (38). This operator, according to NDA and minimal coupling, has a coefficient that is proportional to f^{-2} without any loop suppression. An example is given by the typical four-fermion operator considered in SILH theories that involves only right-hand top quarks:

$$c_{4t}\bar{t}_R\gamma^\mu t_R\bar{t}_R\gamma^\mu t_R. \tag{45}$$

A naive estimation of the coefficient c_{4t} gives $c_{4t} \sim g_s^2/f^2$. A comparison of this operator with the one in Eq. (38), after taking into account the color factors, gives the following identification:

$$|C_1|/3m_t^2 = 1/f^2. \tag{46}$$

In this way, we could directly translate the constraints on the coefficient C_1 into limits on the scale f and the parameter ξ which are comparable to those in Eq. (44). However, this is only possible if we treat all flavors on an equal footing, an assumption that does not apply to most composite models where the coupling to the light quarks is explicitly taken to be different and much suppressed with respect to that of the top quark.

Finally, the limits on $m_\star$ in Eq. (43) imply that the masses of these fermions are close to or larger than 1 TeV. These states are described as custodial fermions because they prevent the mass of the Higgs boson from being too large but this is only true if their masses are less than 1 TeV [10,51].

ACKNOWLEDGMENTS

M. F. is associated with SISSA. He thanks M. Serone for discussions on composite Higgs models and NORDITA in Stockholm for its hospitality during the completion of this work. The work of A. T. was supported by the São Paulo Research Foundation (FAPESP) under Grants No. 2011/11973-4 and No. 2013/02404-1. He thanks G. von Gersdorff for useful discussions and the ICTP Trieste for the hospitality during the completion of this work.

APPENDIX: PARTIAL COMPOSITENESS AND NONMINIMAL COUPLING

In this appendix we introduce an explicit model of partial compositeness to show how the operators in Eq. (6) cannot be rotated away at the tree level by a field redefinition if we assume nonminimal coupling. In the process, we also obtain an estimate of the additional suppression generated by the mixing between composite and SM fermions.

Many realizations of composite Higgs models rely on the hypothesis of partial compositeness [4], in which each SM state has a composite partner with equal quantum numbers under the SM symmetries. These fields are multiples of the global symmetry of the composite sector which can be taken minimally to be $SU(3)_c \times SU(2)_L \times SU(2)_R \times U(1)_X$. We consider here a simplified case in which the composite partners of the top quark are vector-like fermions belonging to the representations $\Psi \sim (2,2)_{2/3}$ and $\tilde{T} \sim (1,1)_{2/3}$ of $SU(2)_L \times SU(2)_R \times U(1)_X$. The multiplet Ψ,

$$\Psi = \begin{pmatrix} T & X_{5/3} \\ B & X_{2/3} \end{pmatrix}, \tag{A1}$$

contains a doublet $Q = (TB)^T$ with the same quantum numbers of the SM left-hand doublet $q_L^{el} = (t_L^{el} b_L^{el})^T$, while $\tilde{T}$ has the same quantum numbers of the SM right-hand top t_R^{el}.

The composite fermion states have an explicit Dirac mass term and are assumed to mix linearly with the SM elementary fields as in the following Lagrangian:

$$\begin{aligned} \mathcal{L}_{\rm mass} + \mathcal{L}_{\rm mix} &= -M_Q \mathrm{Tr}\bar{\Psi}\Psi - M_{\tilde{T}} \bar{\tilde{T}} \tilde{T} - \Delta_Q \bar{Q}_R q_L^{el} \\ &\quad - \Delta_{\tilde{T}} \bar{\tilde{T}}_L t_R^{el} + \mathrm{h.c.} \\ &= -\bar{T}_R (M_Q T_L + \Delta_Q t_L^{el}) - \tilde{T}_L (M_{\tilde{T}} \tilde{T}_R + \Delta_{\tilde{T}} t_R^{el}) \\ &\quad + \mathrm{h.c.} + \ldots \end{aligned} \tag{A2}$$

The mass mixing arising from $\mathcal{L}_{\rm mix}$ can be diagonalized by the following field transformations:

$$\begin{cases} t_L^{el} = \cos\varphi_L t_L + \sin\varphi_L T'_L \\ T_L = -\sin\varphi_L t_L + \cos\varphi_L T'_L \end{cases} \quad \text{and} \quad \begin{cases} t_R^{el} = \cos\varphi_R t_R + \sin\varphi_R \mathcal{T}_R \\ \tilde{T}_R = -\sin\varphi_R t_R + \cos\varphi_R \mathcal{T}_R \end{cases}. \tag{A3}$$

The top fields t_L and t_R are the massless (before EW symmetry breaking) partially composite eigenstates, while T'_L and $\mathcal{T}_R$ are the massive composite ones, their masses being $M_{T'} = M_Q \cos\varphi_L + \Delta_Q \sin\varphi_L$ and $M_{\mathcal{T}} = M_{\tilde{T}} \cos\varphi_R + \Delta_{\tilde{T}} \sin\varphi_R$. The mixing angles φ_L and φ_R are defined such that $\tan\varphi_L = \Delta_Q / M_Q$ and $\tan\varphi_R = \Delta_{\tilde{T}} / M_{\tilde{T}}$.

QCD gauge fields are coupled to the fermions through the covariant derivative $D = \gamma^\mu (\partial_\mu - i g_s T_A G_\mu^a)$ in the kinetic terms

$$\mathcal{L}_{\rm kin} = \bar{q}_L^{el} i \not{D} q_L^{el} + \bar{t}_R^{el} i \not{D} t_R^{el} + \bar{T} i \not{D} T + \bar{\tilde{T}} i \not{D} \tilde{T} + \ldots. \tag{A4}$$

EW interactions are not relevant for our discussion and they are explicitly set to zero. Once the rotation of the fields into the mass eigenstates is performed, using Eq. (A3), the Lagrangian reads

$$\begin{aligned} &\mathcal{L}_{\rm kin} + \mathcal{L}_{\rm mass} + \mathcal{L}_{m\rm mix} \\ &\quad = \bar{t}_L \not{D} t_L + \bar{T}'_L \not{D} T'_L + \bar{t}_R \not{D} t_R + \bar{\mathcal{T}}_R \not{D} \mathcal{T}_R + \bar{T}_R \not{D} T_R \\ &\qquad + \bar{\tilde{T}}_L \not{D} \tilde{T}_L - M_{T'} (\bar{T}_R T'_L + \mathrm{h.c.}) \\ &\qquad - M_{\mathcal{T}} (\bar{\tilde{T}}_L \mathcal{T}_R + \mathrm{h.c.}) + \ldots \end{aligned} \tag{A5}$$

If the composite sector is assumed to be minimally coupled, then the chromomagnetic operator in Eq. (41) can only be generated at loop level (for an explicit example, see Appendix A of [52]). The same holds for the other operator in Eq. (6).

On the other hand, if we allow the composite sector to be nonminimally coupled, then it is possible to introduce the following chromomagnetic interaction term among the composite fermions:

$$\mathcal{L}' = \kappa \bar{Q} H^c \sigma^{\mu\nu} G_{\mu\nu} \tilde{T} + \mathrm{h.c.}, \tag{A6}$$

where H^c is the conjugated composite Higgs field. This operator is suppressed by two inverse powers of the composite fermion mass, namely the coefficient k can be taken to be $\kappa \sim g_s y_t / M_Q^2$, where y_t is the Yukawa coupling of the top quark. After EW symmetry breaking, by performing the rotation Eq. (A3), we obtain

$$\mathcal{L}' = \sin\varphi_L \sin\varphi_R \frac{g_s y_t}{M_Q^2} v \bar{t}_L \sigma^{\mu\nu} G_{\mu\nu} t_R + \mathrm{h.c.} + \ldots, \tag{A7}$$

where the dots stand for other terms which involve the heavy composite fields. A similar argument could be made for the other operator in Eq. (6).

Comparing Eq. (A7) with Eq. (42), we have the following identification:

$$m_*^2 = M_Q^2 / \sin\varphi_L \sin\varphi_R. \tag{A8}$$

Eq. (A8) shows that limits on M_Q turn out to be weaker than those on m_* because of the presence of the suppression factor given by the sine of the mixing angles. However, these mixing angles cannot be too small because they enter into the definition of the top Yukawa coupling, which is generated from the following interaction:

$$\mathcal{L}_{Yuk} = Y^* \bar{Q} H^c \tilde{T} + \mathrm{h.c.}. \tag{A9}$$

Using Eq. (A3), one finds that the top Yukawa coupling is given by

$$y_t = \sin\varphi_L Y^* \sin\varphi_R. \tag{A10}$$

Perturbative control on the strength of the composite interaction requires that $Y^* \lesssim 3$. Then, in order to have $y_t \sim 1$, one needs sizeable mixing angles φ_L and φ_R.

[1] H. Georgi and D. B. Kaplan, Phys. Lett. B **145**, 216 (1984); M. J. Dugan, H. Georgi, and D. B. Kaplan, Nucl. Phys. **B254**, 299 (1985).

[2] K. Agashe, R. Contino, and A. Pomarol, Nucl. Phys. **B719**, 165 (2005).

[3] D. B. Kaplan, Nucl. Phys. **B365**, 259 (1991).

[4] Y. Grossman and M. Neubert, Phys. Lett. B **474**, 361 (2000); T. Gherghetta and A. Pomarol, Nucl. Phys. **B586**, 141 (2000); R. Contino, T. Kramer, M. Son, and R. Sundrum, J. High Energy Phys. 05 (2007) 074.

[5] N. Arkani-Hamed, A. G. Cohen, E. Katz, and A. E. Nelson, J. High Energy Phys. 07 (2002) 034.

[6] E. Farhi and L. Susskind, Phys. Rep. **74**, 277 (1981).

[7] H. Georgi, L. Kaplan, D. Morin, and A. Schenk, Phys. Rev. D **51**, 3888 (1995).

[8] K. Agashe, R. Contino, and R. Sundrum, Phys. Rev. Lett. **95**, 171804 (2005).

[9] G. F. Giudice, C. Grojean, A. Pomarol, and R. Rattazzi, J. High Energy Phys. 06 (2007) 045.

[10] A. Pomarol and J. Serra, Phys. Rev. D **78**, 074026 (2008).

[11] B. Grzadkowski, Z. Hioki, K. Ohkuma, and J. Wudka, Nucl. Phys. **B689**, 108 (2004); B. Lillie, J. Shu, and T. M. P. Tait, J. High Energy Phys. 04 (2008) 087; K. Kumar, T. M. P. Tait, and R. Vega-Morales, J. High Energy Phys. 05 (2009) 022; Z. Hioki and K. Ohkuma, Eur. Phys. J. C **65**, 127 (2010); D. Choudhury and P. Saha, Pramana J. Phys. **77**, 1079 (2011); S. S. Biswal, S. D. Rindani, and P. Sharma, Phys. Rev. D **88**, 074018 (2013).

[12] J. F. Kamenik, M. Papucci, and A. Weiler, Phys. Rev. D **85**, 071501 (2012).

[13] Z. Hioki and K. Ohkuma, Phys. Rev. D **88**, 017503 (2013).

[14] C. Englert, A. Freitas, M. Spira, and P. M. Zerwas, Phys. Lett. B **721**, 261 (2013).

[15] C. Degrande, J.-M. Gerard, C. Grojean, F. Maltoni, and G. Servant, J. High Energy Phys. 03 (2011) 125.

[16] F. J. Ernst, R. G. Sachs, and K. C. Wali, Phys. Rev. **119**, 1105 (1960).

[17] M. Czakon, P. Fiedler, and A. Mitov, Phys. Rev. Lett. **110**, 252004 (2013).

[18] K. Whisnant, J.-M. Yang, B.-L. Young, and X. Zhang, Phys. Rev. D **56**, 467 (1997); J. A. Aguilar-Saavedra, Nucl. Phys. **B812**, 181 (2009).

[19] R. Contino, M. Ghezzi, C. Grojean, M. Muhlleitner, and M. Spira, J. High Energy Phys. 07 (2013) 035.

[20] S. Chen *et al.* (CLEO Collaboration), Phys. Rev. Lett. **87**, 251807 (2001).

[21] J. L. Hewett and T. G. Rizzo, Phys. Rev. D **49**, 319 (1994).

[22] R. Martinez and J. A. Rodriguez, Phys. Rev. D **65**, 057301 (2002); R. Martinez and J. A. Rodriguez, Phys. Rev. D **55**, 3212 (1997).

[23] N. D. Christensen and C. Duhr, Comput. Phys. Commun. **180**, 1614 (2009).

[24] J. Alwall, M. Herquet, F. Maltoni, O. Mattelaer, and T. Stelzer, J. High Energy Phys. 06 (2011) 128.

[25] M. Cacciari, M. Czakon, M. Mangano, A. Mitov, and P. Nason, Phys. Lett. B **710**, 612 (2012).

[26] A. D. Martin, W. J. Stirling, R. S. Thorne, and G. Watt, Eur. Phys. J. C **64**, 653 (2009).

[27] ATLAS Collaboration, Report No. ATLAS-CONF-2012-024.

[28] CMS Collaboration, Report No. CMS-PAS-TOP-11-024.

[29] ATLAS Collaboration, Report No. ATLAS-CONF-2012-134; CMS Collaboration, Report No. CMS-PAS-TOP-12-003.

[30] ATLAS Collaboration, Report No. ATLAS-CONF-2013-097.

[31] CMS Collaboration, Report No. CMS-PAS-TOP-12-007.

[32] CDF Collaboration, CDF Public Note 10926 and D0 Collaboration, D0 Public Note 6363.

[33] G. Aad *et al.* (ATLAS Collaboration), Eur. Phys. J. C **73**, 2261 (2013).

[34] V. Ahrens, A. Ferroglia, M. Neubert, B. D. Pecjak, and L. L. Yang, J. High Energy Phys. 09 (2010) 097.

[35] T. Sjostrand, S. Mrenna, and P. Z. Skands, J. High Energy Phys. 05 (2006) 026.

[36] CDF Collaboration, CDF Public Note 9602.

[37] CMS Collaboration, Reports No. CMS-TOP-12-027 and No. CMS-TOP-12-028.

[38] W. Bernreuther and Z.-G. Si, Phys. Lett. B **725**, 115 (2013).

[39] The ATLAS Collaboration, Report No. ATLAS-CONF-2013-101.

[40] I. Sick, Phys. Lett. B **576**, 62 (2003).

[41] D. Bourilkov, Phys. Rev. D **64**, 071701 (2001).

[42] G. Gabrielse, D. Hanneke, T. Kinoshita, M. Nio, and B. C. Odom, Phys. Rev. Lett. **97**, 030802 (2006); **99**039902 (2007).

[43] M. Ciuchini, E. Franco, S. Mishima, and L. Silvestrini, arXiv:1306.4644; C. Grojean, O. Matsedonskyi, and G. Panico, J. High Energy Phys. 10 (2013) 160.

[44] E. Eichten, K. D. Lane, and M. E. Peskin, Phys. Rev. Lett. **50**, 811 (1983).

[45] F. Bazzocchi, U. De Sanctis, M. Fabbrichesi, and A. Tonero, Phys. Rev. D **85**, 114001 (2012).

[46] O. Domenech, A. Pomarol, and J. Serra, Phys. Rev. D **85**, 074030 (2012).

[47] G. Aad *et al.* (ATLAS Collaboration), Phys. Lett. B **694**, 327 (2011); V. Khachatryan *et al.* (CMS Collaboration), Phys. Rev. Lett. **106**, 201804 (2011).

[48] A. Manohar and H. Georgi, Nucl. Phys. **B234**, 189 (1984); H. Georgi and L. Randall, Nucl. Phys. **B276**, 241 (1986).

[49] E. E. Jenkins, A. V. Manohar, and M. Trott, J. High Energy Phys. 09 (2013) 063.

[50] K. Agashe, R. Contino, L. Da Rold, and A. Pomarol, Phys. Lett. B **641**, 62 (2006).

[51] G. Panico, M. Redi, A. Tesi, and A. Wulzer, J. High Energy Phys. 03 (2013) 051; R. Contino, L. Da Rold, and A. Pomarol, Phys. Rev. D **75**, 055014 (2007).

[52] M. Redi, V. Sanz, M. de Vries, and A. Weiler, J. High Energy Phys. 08 (2013) 008.